How to cite: *Angew. Chem. Int. Ed.* **2024**, *63*, e202318283
doi.org/10.1002/anie.202318283

Mesoionic Compounds

Pyridinium-Derived Mesoionic *N*-Heterocyclic Olefins (py-mNHOs)

Qiu Sun, Andreas Eitzinger, Robin Esken, Patrick W. Antoni, Robert J. Mayer, Armin R. Ofial,* and Max M. Hansmann**

Abstract: Mesoionic polarization allows access to electron-rich olefins that have found application as organocatalysts, ligands, or nucleophiles. Herein, we report the synthesis and characterization of a series of 3-methylpyridinium-derived mesoionic olefins (py-mNHOs). We used a DFT-supported design concept, which showed that the introduction of aryl groups in the 1-, 2-, 4-, and 6-positions of the heterocyclic core allowed the kinetic stabilization of the novel mesoionic compounds. Tolman electronic parameters indicate that py-mNHOs are remarkably strong σ-donor ligands toward transition metals and main group Lewis acids. Additionally, they are among the strongest nucleophiles on the Mayr reactivity scale. In reactions of py-mNHOs with electron-poor π-systems, a gradual transition from the formation of zwitterionic adducts via stepwise to concerted 1,3-dipolar cycloadditions was observed experimentally and analyzed by quantum-chemical calculations.

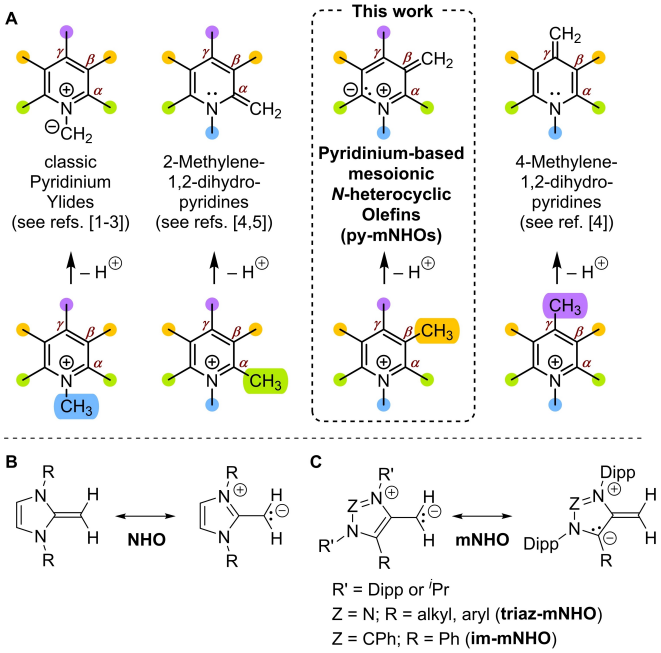

Figure 1. (A) Deprotonation of methyl-substituted pyridinium ions yields ylides or mesoionic *N*-heterocyclic olefins and 2- or 4-methylene-dihydropyridines. (B) Established NHOs and (C) mesoionic NHOs (mNHOs). Dipp: 2,6-diisopropylphenyl.

Introduction

Deprotonation of *N*-alkylated pyridinium salts at the N–R group to give pyridinium ylides (Figure 1A) is an often-used strategy to generate nucleophiles or 1,3-dipoles that undergo further reactions with electron-poor reaction partners to form, for example, Michael adducts, heterocyclic (3+2)-cycloadducts, or cyclopropanes.[1] The reactivity of such classic pyridinium ylides can be estimated by reference to reported pK_a values[2] and Mayr nucleophilicity parameters.[3]

Base-activation of methyl groups at the α- and γ-ring positions of *N*-alkylated pyridinium ions is feasible under relatively mild conditions and frequently used in Knoevenagel-type condensations with aldehydes to yield molecules with extended π-systems.[4] Furthermore, 2-methylene-1,2-dihydropyridines have recently been utilized in addition reactions to Michael acceptors and heterocumulenes, as ligands for metal complexes, and for synthetizing diazoalkenes by diazo-transfer from azides.[5]

In contrast, deprotonation of β-methyl groups in *N*-alkylpyridinium ions is expected to generate thermodynamically disfavored mesoionic molecules. Mesoionic compounds are neutral molecules but require zwitterionic Lewis structures with mutually conjugated formal negative and positive charges.[6,7]

In 2020, the Hansmann group introduced mesoionic polarization as a new concept to generate strongly polarized

[*] Dr. Q. Sun, M. Sc. R. Esken, M. Sc. P. W. Antoni, Prof. Dr. M. M. Hansmann
Fakultät für Chemie und Chemische Biologie, Technische Universität Dortmund
Otto-Hahn-Str. 6, 44227 Dortmund (Germany)
E-mail: max.hansmann@tu-dortmund.de
Dr. A. Eitzinger, Dr. A. R. Ofial
Department Chemie, Ludwig-Maximilians-Universität München
Butenandtstr. 5–13 (Haus F), 81377 München (Germany)
E-mail: ofial@lmu.de
Dr. R. J. Mayer
Institut de Science et d'Ingénierie Supramoléculaires (ISIS), CNRS UMR 7006, Université de Strasbourg
8 Allée Gaspard Monge, 67000 Strasbourg (France)
E-mail: rjmayer@unistra.fr

olefins with exocyclic methylene (=CH_2) groups.[8] Such mesoionic compounds show increased C–C bond polarization compared to well-established *N*-heterocyclic olefins (NHOs; Figure 1B), which have proven to be potent organocatalysts, nucleophiles, and Lewis bases.[9–12] The initially investigated mesoionic *N*-heterocyclic olefins (mNHOs) were derived from triazolium (triaz-mNHO) and imidazolium salts (im-NHOs) (Figure 1C). Kinetic studies showed that triaz-mNHOs are highly nucleophilic,[13] and easily activate inert small molecules such as nitrous oxide to furnish stable diazoalkenes.[14] Recently, mNHOs have proven their potency as organocatalysts[15] and in coordination chemistry.[16–18]

Given that mesoionic methylides with unsubstituted = CH_2 groups are rare,[19] the structures that result from deprotonating the β-methyl group of pyridinium precursors attracted our attention. Herein, we introduce pyridinium-derived mNHOs as a new class of six-membered mesoionic methylides. A DFT-guided design concept enabled us to prepare and characterize a series of stable but highly reactive py-mNHOs. Further, we define the reactivities of py-mNHOs toward various electron-deficient reaction partners by synthetic, kinetic, and quantum-chemical studies and propose a method for predicting nucleophilic reactivities of novel py-mNHOs.

Results and Discussion

Electronic Structure and Stability of py-mNHOs

We started with a computational analysis of the three parent *N*-methyl pyridine isomers **I–III** with methylene-substituents at the α-, β-, and γ-ring positions (Figure 2; for full details and references to the computational methods, see part 3 of the Supporting Information). While the α- and γ -isomers **I** and **III** are energetically nearly equal, the mesoionic isomer **II** is significantly higher in energy (+75 kJ mol^{-1}), indicating a challenge in synthetically accessing this class of mesoionic compounds.

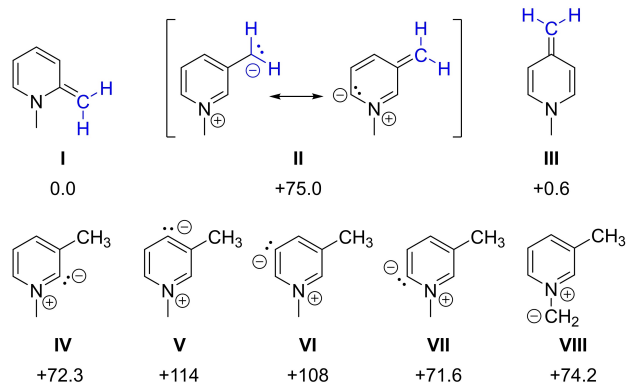

Figure 2. Comparison of the relative Gibbs free energies in kJ mol^{-1} of the parent zwitterionic pyridine isomers C_7H_9N at the SMD(THF)/ωB97X–D/def2-TZVP//SMD(THF)/B3LYP–D3BJ/def2-SVP level of theory.

We further considered the relative energies for the isomeric structures that could originate from the deprotonation of different sites at the pyridinium ring (**IV–VII**). Interestingly, the *N*-heterocyclic carbenes **IV** and **VII** are even lower in energy (+72.3 kJ mol^{-1} and +71.6 kJ mol^{-1}) than the olefin **II** (+75 kJ mol^{-1}), suggesting the necessity to substitute the 2- and 6-positions.[20] Note, that in **II** the negative charge is delocalized within the π-system, while for the *N*-heterocyclic carbenes (**IV–VII**) it is located (and not delocalized) in the plane of the heterocyclic ring. Also, the energy for *N*-methyl deprotonation to give the pyridinium ylide **VIII** (74.2 kJ mol^{-1}) is comparable to that of the desired mesoionic olefin **II**, suggesting *N*-arylation to avoid *N*-alkyl deprotonation pathways.[21]

On this basis, we designed **1a** as a possible target molecule for our studies on py-mNHOs (Figure 3A). In **1a**, *N*-arylation is combined with bearing another three phenyl substituents in the 2-, 4-, and 6-positions of the pyridinium ion. Symmetrical 3,5-dimethylation of the precursor should then allow selective access to py-mNHO **1a** by deprotonating one of the methyl groups through a sufficiently strong Brønsted base.

Next, we compared the electronic structures of the aryl-protected target **1a** and the parent py-mNHOs **II** computationally (Figure 3). Analysis of the frontier molecular orbitals indicated full delocalization between the methylene unit and the pyridine core in both molecules (Figure 3A). The substituents introduced to stabilize **1a** with respect to **II** did not change the shape of the HOMO, and only minor delocalization into the phenyl rings at ring positions 2 and 6 was seen in the LUMO. The delocalized nature of **II** was further corroborated by a natural resonance theory (NRT) analysis,[22] which illustrated the mesoionic nature of the py-mNHO system (Figure 3B shows structures with a sum of 61.3 %).

We then analyzed to which extent the aromaticity of the pyridinium core in **II** or **1a** remains conserved. To study the magnetic criterium for aromaticity, NICS(1)$_{zz}$-scans (distance from plane 1 Å) were performed on the three different isomers **I–III**, **1a**, and the unsubstituted *N*-methylpyridinium ion (Figure 3C).[23] The comparison of these species indicates that the py-mNHOs either display no significant magnetic shielding or deshielding (**I**, **III**) or show moderate paratropicity (**I**, **1a**). In contrast, significant diatropicity is observed for the aromatic *N*-methyl-pyridinium ion itself. Paratropicity is typically associated with antiaromaticity. However, further analysis of the aromaticity of **II** by homodesmotic reactions indicates significant resonance stabilization of the methylene or butadiene unit (Figure 3D).[24] In analogy to other mesoionic compounds, py-mNHOs, like **II** or **1a**, might be best described as non-aromatic. The formation of an aromatic pyridinium heterocycle through the reaction of the exocyclic methylene group with an electrophile could thus contribute significantly to the thermodynamic driving force for reactions of the py-mNHOs.

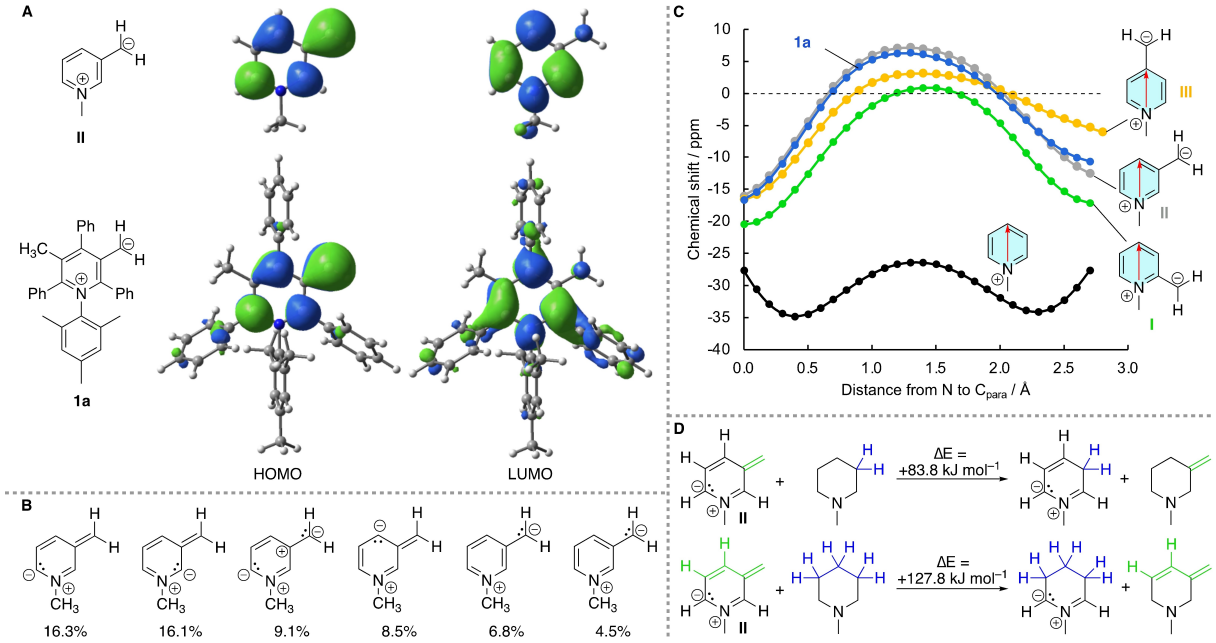

Figure 3. Analysis of the electronic structure of py-mNHOs. (A) Frontier molecular orbitals of the parent py-mNHO **II** and **1a** at the SMD(THF)/B3LYP–D3BJ/def2-SVP level of theory. (B) Most relevant resonance structures for py-mNHO **II** according to a natural resonance theory (NRT) analysis (C) NICS(1)$_{zz}$-scans (distance from plane 1 Å) for the structures **I–III**, **1a**, and the *N*-methylpyridinium ion. (D) Homodesmotic reactions to evaluate the resonance stabilization energy of **II**.

Synthesis of pyridinium-derived mNHOs (py-mNHOs)

We began our experimental study by preparing *N*-aryl-3,5-dimethyl-2,4,6-triphenyl-pyridinium tetrafluoroborates **1′a–d** from anilines and 3,5-dimethyl-2,4,6-triphenylpyrylium tetrafluoro-borate, accessible in a multi-gram scale from propiophenone in a single step[25] (Scheme 1). Upon addition of potassium bis(trimethylsilyl)-amide (KHMDS, 1.1 equiv.) to a suspension of pyridinium salts **1′a–d** in THF at −40 °C, an instant change from colorless to deep green solutions was observed. By crystallization from the reaction mixture at −40 °C for 24 h, mesoionic pyridine olefins (py-mNHOs) **1a–d** could be isolated as deeply green, crystalline solids in yields of 51–77 %. The intense colors originate from a HOMO–LUMO transition in agreement with TD-DFT calculations (see Figures S116–S121). Compounds **1a–d** are stable at room temperature in the solid-state under an inert atmosphere for at least 24 h. The lifetime of **1** in solution strongly depended on the *N*-aryl fragment. The (4-trifluoromethylphenyl)-substituted **1d** degraded faster than the other py-mNHOs, while the *N*-mesityl fragment in **1a** significantly increased its lifetime in solution (see Figures S23–S26 in the SI).

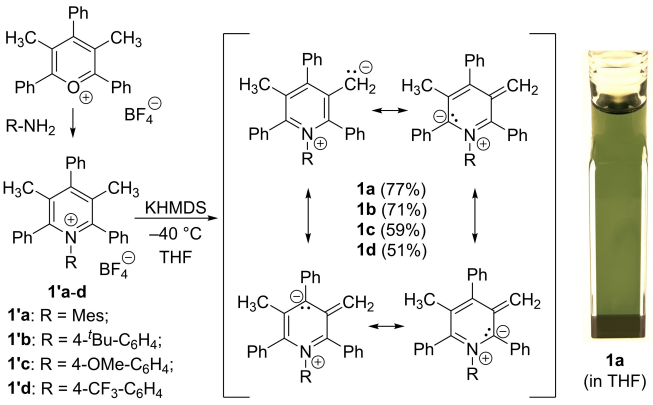

Scheme 1. Synthesis of mesoionic pyridine-derived *N*-heterocyclic olefins **1a–d**. Right: photo of a cuvette filled with a dilute solution of **1a** dissolved in THF at rt.

The ^{1}H NMR spectra of **1a–d** in d$_8$-THF (at −30 or −20 °C) show two strongly high-field shifted resonances in a range from δ = 2.44 to 2.39 ppm for the exocyclic methylene protons, which agrees with hindered rotation around the C=CH$_2$ bond. The slight signal broadening is caused by small absolute values in the geminal $^2J_{HH}$ coupling constants (< 2 Hz). The chemical shift range agrees with olefin signals observed for mNHOs, which are typically in the range from δ = 2.0 to 3.6 ppm.[8] The ^{13}C NMR signals of the exocyclic methylene carbon atoms (=CH$_2$) of **1a–d**, however, resonated more high-field shifted (δ = 74.5–75.9 ppm) than normal olefins but remarkably low field-shifted compared to NHOs or mNHOs (δ = 40.2–51.8 ppm; for a summary of ^{13}C NMR shifts, see Figure S79 in the SI).

For **1a** and **1b**, we obtained crystals from a THF/pentane solution at −40 °C suitable for single crystal X-ray analysis. The solid-state structures supported the formation of py-mNHOs as a novel class of mesoionic mNHOs (**1b** is shown in Figure 4; the solid-state structure of **1a** features nearly identical bond parameters, see Figure S81 in the SI).[26] In the solid-state structure of **1b**, the C3–C7 [1.411(1) Å] and C5–C8 [1.474(1) Å] bond lengths are both shortened

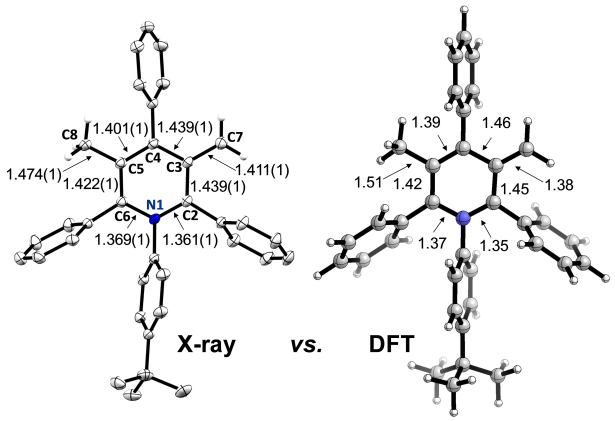

Figure 4. Comparison between X-ray solid-state structure of **1b** (left) and DFT (SMD(THF)/B3LYP–D3BJ/def2-SVP) optimized structure (right). Thermal ellipsoids are shown with 50% probability. Selected bond lengths are shown in [Å].

compared to the corresponding C–C distances for C–CH_3 [1.506(2)/1.503(2) Å] in the symmetrical pyridinium salt **1′b**. A reliable determination of the C–CH_2 bond length in the solid-state is difficult due to the negligible topological difference of CH_2 vs. CH_3, resulting in a superposition of both orientations (in **1b**, one orientation is slightly preferred with a 71:29 ratio). The DFT calculations reveal more clearly the different bond lengths: The C3–CH_2 bond (1.38 Å) is significantly shorter than the C5–CH_3 bond (1.51 Å) (Figure 4).

For **1b**, a degradation pathway was experimentally identified (Scheme 2). Keeping a solution of the py-mNHO **1b** in benzene at room temperature for two days led to the slow formation of a dimer $(\mathbf{1b})_2$, a formal (3+3) dimerization product (Scheme 2), which was verified by X-ray solid-state structure analysis. $(\mathbf{1b})_2$ was formed by nucleophilic attack on the electrophilic C2 position of the pyridine core. The solid-state structure confirms a *cis*-orientation of the two phenyl groups at the central six-membered ring in an overall C_2-*trans*-symmetric structure.

According to DFT calculations, the formation of the dimer $(\mathbf{1b})_2$ from **1b** is strongly exergonic with $\Delta G = -174\ kJ\,mol^{-1}$, and the dimerization is thus irreversible. In agreement, attempts to liberate the monomer from the dimer in d_8-THF at 80 °C in a closed NMR tube and trapping it were not successful (see Figure S22 in the SI). Computational analysis of the dimerization of the model system **P1** indicates that dimerization is energetically possible via various low-lying transition states that can yield different isomers via both concerted or stepwise pathways (see SI, Figure S109 for an overview). As the dimerization for the unsubstituted model **P1** and the experimentally investigated species **1** is computed to show similar exergonicity, the aryl substituents predominantly stabilize **1** kinetically.

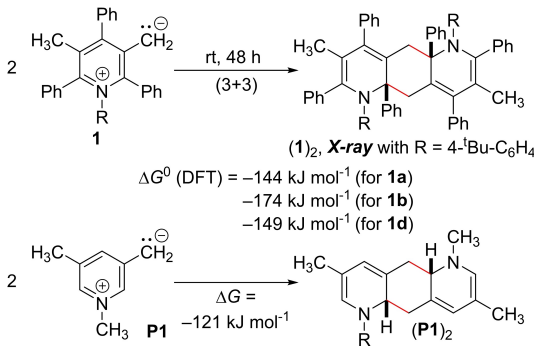

Scheme 2. The py-mNHOs **1** degrade in solution by (3+3)-cycloadditions to furnish the thermodynamically more stable dimers $(\mathbf{1})_2$. Bottom: Energetics for the dimerization of the model compound **P1** (for possible transition states of the dimerization, see Figure S109 in the SI). Energies were calculated at the SMD(THF)/ωB97XD/def2-TZVP//SMD(THF)/B3LYP–D3BJ/def2-SVP level of theory.

Reactivity of py-mNHOs—Novel 1,3-Dipoles

We next investigated the reactivity of the py-mNHOs. For practical reasons we selected the most stable derivative **1a** for the reactivity studies. The reaction of **1a** with the Lewis acid $B(C_6F_5)_3$ gave the colorless Lewis adduct **2** (yield: 85%), which could be characterized by X-ray analysis (Scheme 3). The solid-state structure verified the end-on binding mode by the exocyclic methylene group to boron, similar to the adducts previously reported for mNHOs.[8] In solution, **2** features NMR resonances (243 K) at $\delta(^{11}B) = -13.1$ ppm [^{11}B ($\nu_{1/2} \approx 30$ Hz)] and $\Delta\delta(^{19}F_{m,p})$ chemical shift difference of 3.3 ppm, which is typical for tetracoordinated boron and in good agreement with the solid-state derived structural assignment.

Subsequently, applications of py-mNHOs in carbon-carbon bond-forming reactions with electron-deficient π-systems were investigated (Scheme 3). When arylidene malonate **3c** reacted with **1a** in THF at −40 °C, the reaction mixture instantaneously turned from deep green to colorless upon the last drop of **3c**, indicating a highly reactive mesoionic system. The product was identified by X-ray solid-state structure determination as the (3+2) cycloadduct **6a** containing a cyclopenta[*c*]dihydropyridine core (yield: 83%). The formation of cycloadducts by py-mNHOs contrasts with the reactivity of triazole- or imidazole-derived mNHOs, which showed exclusively σ-type reactivity of the exocyclic methylene group in reactions with Michael acceptors.[8,13] In **6a**, the phenyl group at the 4-position and the aryl group from the dipolarophile are exclusively *trans*-oriented. Most strikingly, in situ experiments of the reaction of **1a** with **3c** in d_6-benzene almost quantitatively led to diastereomerically pure **6a** (d.r. >99:1; for further details, see Figure S31 in the SI).

Also, ethyl cinnamate (**4**) and butyl acrylate (**5**) showed excellent reactivity towards **1a**, leading to diastereomerically pure **6b** and **6c** in high yields of 89% and 81%, respectively. To investigate whether the cycloadditions occurred via concerted or stepwise mechanisms, we utilized *E* and *Z*-configured olefins as stereochemical probes. Both dimethyl maleate (**7**) and dimethyl fumarate (**8**) furnished the (3+2)

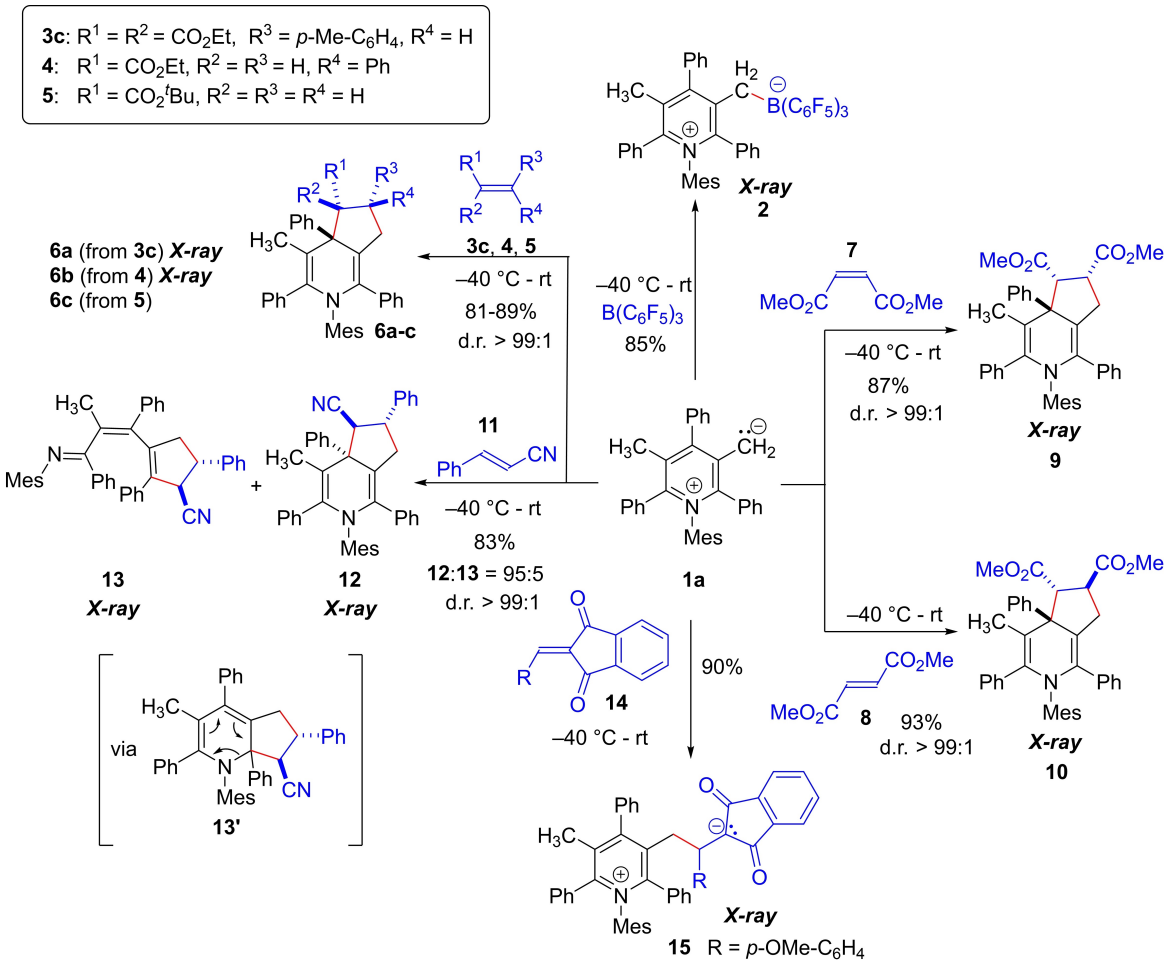

Scheme 3. Reactivity of py-mNHO **1a** as nucleophiles as well as 1,3-dipoles.

cycloaddition products **9** (yield: 87 %) and **10** (yield: 93 %), respectively, which were fully characterized by spectroscopic methods. In situ NMR spectra agreed with the isolated products, for which exclusive formation of *cis*-**9** and *trans*-**10** was observed.[27] The relative stereochemistry could be unambiguously assigned by X-ray diffraction. Controlled by the preferred *trans*-configuration between the pyridine's 4-phenyl and the vicinal ester group, three adjacent stereocenters are formed concomitantly. Since *E*- and *Z*-configured olefins cleanly generated *cis*-**9** and *trans*-**10**, respectively, the maintained stereochemical information supports a concerted mechanism of the 1,3-dipolar cycloaddition.

The observed high stereoselectivity might result from steric repulsion between the ester and the 4-phenyl groups. To investigate dipolarophiles with less voluminous acceptor groups, we selected cinnamonitrile (**11**). Surprisingly, in this case, a 95:5 mixture of **12** and **13** was isolated (total yield: 83 %). In situ NMR analysis showed a similar **12:13** selectivity, while no intermediate could be detected. The structures of **12** and **13** could be verified by X-ray diffraction. The bicyclic, diasteromerically pure main product **12** was characterized as the *trans*-configured (3+2) cycloadduct. The formation of **13** can be explained via initial (3+2) cycloaddition involving the 2-position instead of the 4-position of the pyridine ring (intermediate **13′**), which is presumably followed by electrocyclic C–N bond cleavage of the heterocycle to furnish the open α,β,γ,δ-unsaturated imine **13**.[28]

Next, the reaction of indandione methide **14** with py-mNHO **1a** in toluene was investigated and shown to furnish the zwitterion **15** (yield: 90 %), in which the indan-1,3-dione moiety efficiently stabilizes the negative charge. The product was analyzed by NMR spectroscopy as well as by X-ray diffraction. Products of competing 1,3-dipolar cycloadditions were not detected. Even upon heating a solution of zwitterion **15** in d_6-benzene at 80 °C for several hours, the NMR spectra of the sample did not show any indication of the formation of a cyclized product.

Additionally, the scope of the dipolarophiles was widened from C=C double bonds to π-systems with heteroatoms such as N=N and C=O bonds (Scheme 4). Diisopropyl azodicarboxylate (**16**) reacted smoothly with py-mNHO **1a** to give (3+2) cycloaddition product **17** (yield: 91 %), which was fully characterized, including analysis by X-ray diffraction. The X-ray structure confirms the product to arise from a ring closure across the 3-CH_2 group and the 4-position of the pyridine core.

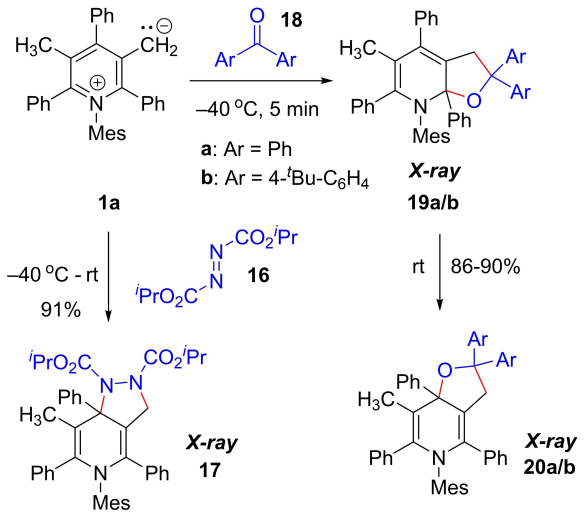

Scheme 4. Reactivity towards diazo and carbonyl-electrophiles.

Benzophenones (**18**) with different substitution patterns were next investigated. Initially, we successfully isolated the expected (3+2) cycloaddition products **20a** and **20b** arising from a 1,3-dipolar reactivity across the (3-CH_2→4)-positions of the pyridine core in high yields (90 % for **20a** in 12 h and 86 % for **20b** in 72 h; Scheme 4). Surprisingly, upon in situ monitoring of the reaction progress by ^{1}H NMR spectroscopy at −40 °C, the formation of intermediates **19a/b** could be detected, which selectively rearranged into **20a/b** (see Supporting Information). Notably, electron-donating substituents on the benzophenone decreased the rate for the rearrangement from **19b** to **20b** compared to **19a**/**20a**. In both cases, we could isolate the intermediates **19** in moderate yields (63 % and 65 %) and characterize them at −40 °C by NMR spectroscopy. Crystalline **19b** could be obtained in THF/pentane solution at −40 °C, whose X-ray analysis confirmed a 1,3-dipolar cycloaddition across the (3-CH_2→2)-positions of the pyridine core (see SI, Figure S93).

Calculations at the SMD(THF)/ωB97X–D/def2-TZVP//SMD(THF)/B3LYP–D3BJ/def2-SVP level of theory indicate that the (3-CH_2→4)-cycloaddition products **20** are the thermodynamically favored products. Interestingly, in the (3-CH_2→2)-cycloaddition product **19**, the electrocyclic ring opening, as observed for **13′**→**13**, does not seem to occur, and instead, the C–O bond of the N,O-acetal unit is broken. DFT calculations could not confirm the existence of a zwitterionic intermediate, and C–O bond breakage only leads to a flat region on the energy surface from which subsequent cyclization to the other isomer presumably occurs (for DFT calculations comparing the different reaction pathways, see Table S13 and Figure S115).[29]

Concerted vs. Stepwise (3+2) Cycloaddition

The cycloaddition experiments with dimethyl maleate (**7**) and dimethyl fumarate (**8**) resulted in exclusively *cis* and *trans*-configured products supporting a concerted mechanism of the 1,3-dipolar cycloaddition.[30] In contrast, experiments with the benzylideneindan-1,3-dione (**14**) to give the open adduct **15** and with $B(C_6F_5)_3$ to give **2** confirmed an initial attack of the exocyclic 3-CH_2 group at the Michael system or the boron-centered Lewis acid, respectively, with the formation of zwitterionic products. To get more insight into the mechanism of the (3+2) cycloaddition, we quantum-chemically investigated the reaction between **1a** and electrophiles/dipolarophiles with different electronic properties.

Initially, the mechanism of the reaction of **1a** with cinnamonitrile (**11**) was computationally studied. The reaction of these substrates was computed to proceed via rate-limiting C–C bond formation between the exocyclic methylene group of **1a** and the Michael acceptor **11** via TS1 (Figure 5A), which, due to hindered rotation, can pass through two different rotamers $TS1_{RotA}$ or $TS1_{RotB}$. Depending on the specific conformer for $TS1_{RotA}$ or $TS1_{RotB}$, the cycloadduct can be formed directly via an asynchronous concerted/two-step no-intermediate mechanism or through a zwitterionic intermediate (see insert in Figure 5A for the 3D structure of the lowest conformer for TS1). In cases where intermediates were observed, only a small subsequent barrier via TS2 could be observed. Due to the reaction proceeding either by an asynchronous concerted pathway or via a small barrier in TS2, the regio- and diastereoselectivity is set by the orientation and conformation of the substrates at the transition state TS1. Further analysis of the potential energy surface for the reaction of **1a** with **11** confirmed this interpretation. After forming the first C–C bond through conjugate addition of the methylene unit of **1a** at **11**, the reaction coordinate points to a flat region on the potential energy surface, from where the product is attainable. Despite these insights, our computational model could not correctly reproduce the experimentally observed selectivity for forming the 1,4-product due to the small energetic differences and the errors associated with the methods, and the lowest computed transition state instead leads to the 1,2-product.

An analogous mechanism as with **11** was computed for the reaction of **1a** with dimethyl maleate (**7**), which gives zwitterionic intermediates via TS1, whose barriers for cyclization via TS2 are so low (≈5–10 kJ mol^{-1}) that both regio- and diastereoselectivity are again already determined by the orientation of the reactants in TS1, the transition state of the bond-formation resulting from conjugate addition between the exocyclic methylene group of **1a** and the Michael acceptor **7** (see SI, Figure S112). We could not localize intermediates in our computations for the reaction of **1a** with benzophenone (**18a**), and all transition states directly led to cycloadducts **19** or **20**. However, due to the similarity of the computed activation barriers and the associated error limits, we could not reproduce the kinetic preference for the formation of **19** over **20**.

Finally, we computed the mechanism for the reaction of **1a** with benzylidene malonate (**3b′**), which features two acceptor groups able to stabilize the zwitterionic intermediates (Figure 5B). For this system, the energy of the zwitterionic intermediate is lowered relative to the reactants,

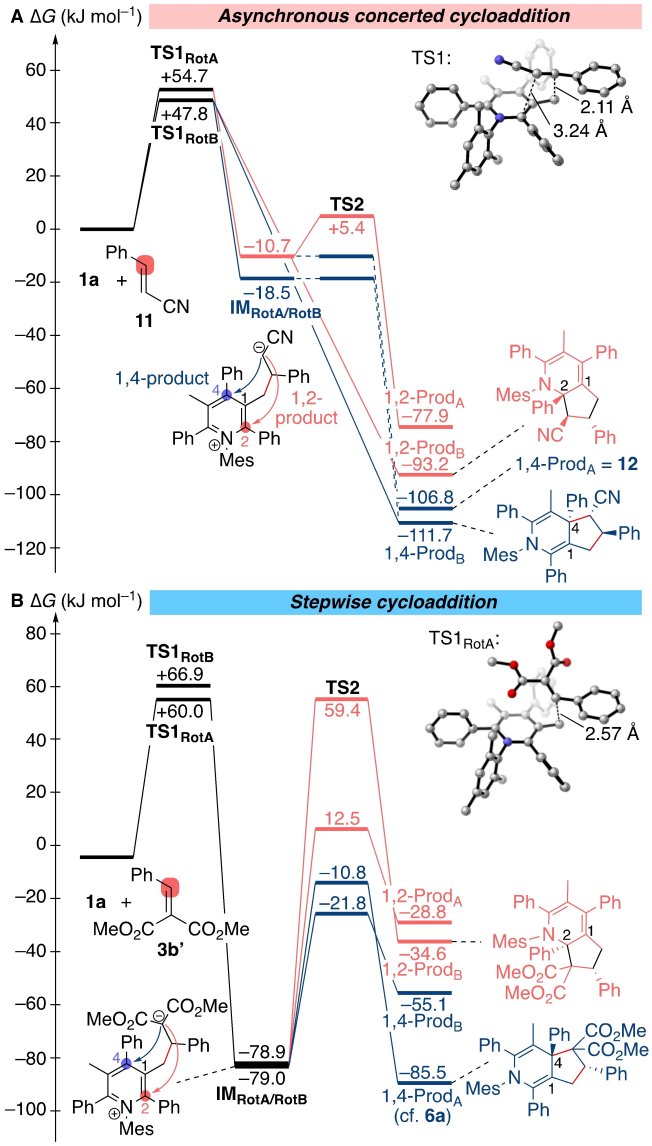

Figure 5. Gibbs energy profile for (A) the concerted 1,3-dipolar cycloaddition of **1a** with **11** and (B) the analogous stepwise reaction of **1a** with **3b′**. For efficient computations at the SMD(THF)/ωB97X–D/def2-TZVP//SMD(THF)/B3LYP–D3BJ/def2-SVP level of theory, the ethyl groups of **3b** were replaced by methyl groups in **3b′**. All energy values correspond to Boltzmann-weighted averages for ensembles of conformers. For each reaction, only the energetically more favorable diastereomers ($Prod_A$ or $Prod_B$) for each regioisomeric product (1,2- or 1,4-product, see the Figure for the definition of these numbers) are depicted. For the full energy profiles and details on the computations, see Figures S111 and S113 in the SI.

and a significantly larger barrier for subsequent ring closure via TS2 is observed. Computations indicate that cyclization to yield the 1,2-cycloaddition products is kinetically unfavored. Cyclization to the 1,4-products is kinetically significantly more favorable, and the stereoisomer corresponding to the experimentally isolated product resembles the thermodynamic product of the reaction. Again, the potential energy surface was quantitatively evaluated (Figure S110). In contrast to the surface computed for the reaction of **1a** with **11**, the zwitterionic intermediate corresponds to a local minimum on the potential energy surface with **3b′**.

Further increasing the stabilization of the zwitterionic intermediate fully inhibits ring closure, as experimentally observed in the reaction of **1a** with indandione **14** and computationally verified by the zwitterionic adduct being by 19.5 kJ mol^{-1} more stable than the corresponding cycloadduct.

Donor Properties, Brønsted Basicities and Nucleophilicities

Tolman electronic parameters (TEP). After assessment of the reactivity of the py-mNHOs, we experimentally quantified their overall donor properties. For this purpose, the rhodium carbonyl complex **21** was prepared by reacting **1a** with rhodium carbonyl dimer $[Rh(CO)_2Cl]_2$ (Scheme 5).

The end-on binding mode by the exocyclic methylene carbon to rhodium in **21** (yield: 90 %) could be structurally verified by X-ray diffraction (Figure 6).[26] IR stretching frequencies of the Rh-complex **21** were measured to characterize the overall donor property of the corresponding

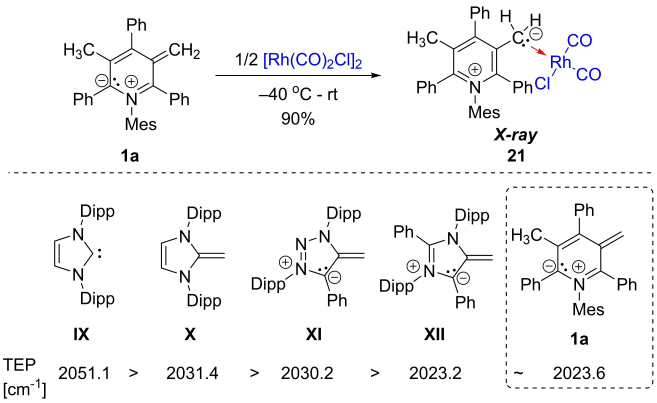

Scheme 5. Top: Preparation of the rhodium complex **21**. Bottom: Selected TEP values of strong carbon donors from ref. [8].

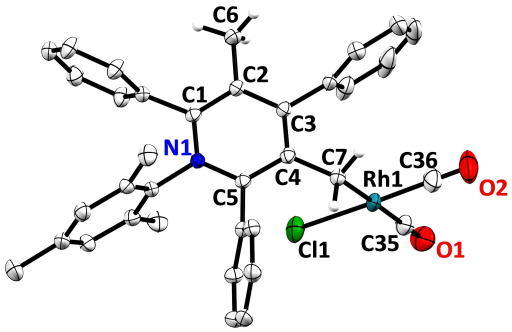

Figure 6. X-ray solid-state structure of rhodium complex **21**. Thermal ellipsoids are shown with 50% probability. Hydrogen atoms (except $-CH_3$ and $-CH_2$) were omitted for clarity. Selected bond parameters in [Å] and [°]: N1–C1 1.365(2), C1–C2 1.390 (2), C2–C3 1.400(2), C3–C4 1.409(2), C4–C5 1.405(2), N1–C5 1.372(2), C2–C6 1.507(2), C4–C7 1.478(2), Rh1–C7 2.155(1), Rh1–C35 1.893(2), Rh1–C35 1.825(2), C5–C4–C7 122.0(1), C3–C4–C7 120.5(1), C4–C7–Rh1 110.9(1).

olefin **1a** by the Tolman electronic parameter (TEP).[31] Solution (CH_2Cl_2) phase IR bands of **21** are at ν = 2044.6 cm^{-1} and 1964.0 cm^{-1} (ν_{av} = 2004.3 cm^{-1}) and allow to derive a TEP value according to TEP = 0.8001 ν_{av} + 420 cm^{-1},[31] of **1a** to be 2023.6 cm^{-1}, which represents an exceptionally strong donor exceeding strong carbon donors such as IPr carbene (**IX**), NHO (**X**) and triaz-mNHOs (**XI**) (Scheme 5).[8] The TEP of **1a** is one of the lowest TEP values reported and very close to the one of the so far strongest donor, the imidazole-derived mNHO **XII** (Scheme 5).[8]

Additionally, the metal-ligand binding affinity was evaluated by ligand-exchange reactions at the L(Rh(CO)$_2$Cl complex. Upon mixing **21** with mNHO **XI** in a 1:1 ratio in d_8-THF a 1:2 mixture of free py-mNHO **1a** and triaz-mNHO **XI** as well as the corresponding rhodium complexes was observed. Addition of carbene **IX** to **21** liberated py-mNHO **1a** and generated the carbene-rhodium complex (for more information, see Figure S75–78). The formation of the carbene complex can be attributed to the thermodynamically more stable C–Rh bond due to π-backdonation, similar to the previously observed ligand exchange reactions with triaz-mNHOs.[8]

Brønsted basicity. We then investigated the Brønsted basicity of **1a** relative to triaz-mNHO **XI** (Scheme 6). Upon addition of **1a** to a THF solution of the triazolium salt **22**-PF_6 we could observe an instant color change from green to purple and detect by ^{1}H NMR spectroscopy the quantitative formation of triaz-mNHO **XI** and pyridinium salt **1′a**-PF_6. Hence, it can be concluded that the overall donor properties and the basicity of the new py-mNHOs **1** outperform those of the previously reported triaz-mNHOs (*N*-Dipp).

Kinetics of the reactions of py-mNHO with Michael acceptors. We recently observed that the TEP value is not a good indicator to quantify the nucleophilicities of mesoionic olefins.[13] Therefore, we targeted the quantification of the nucleophilicity of **1a** by kinetic measurements to locate the position of **1** on the well-established Mayr scale.[32] Beneficially, Mayr's nucleophilicity scale already comprises entries for classical NHOs[11] and triaz-mNHOs,[13] which facilitates embedding **1a** in a context of structurally related nucleophiles.

Given that DFT calculations indicated a stepwise mechanism for the reactions of **1a** with arylidenemalonates **3** (see above), we selected this class of Michael acceptors as reference electrophiles for kinetic measurements. Arylidenemalonates **3a**–**3e** were previously suggested as reference electrophiles for the characterization of highly reactive nucleophiles. Substituent variation at the aromatic ring modulates the electrophilicity over five orders of magnitude, as defined by the electrophilicities *E* in Mayr's linear free energy relationship (1).[33]

$$\lg k_2(20\,^{\circ}\mathrm{C}) = s_N(N + E) \quad (1)$$

The reactivity of a given nucleophile, such as **1a** (in THF), is described by two solvent-dependent parameters in equation (1): the nucleophilicity *N* and the sensitivity s_N. The kinetics of the reactions of **1a** with **3a–e** were recorded in THF at 20 °C by stopped-flow methods following the decay of the absorption of **1a** at λ = 625 nm photometrically. The electrophiles, which are transparent at this wavelength, were used in excess, that is, $[\mathbf{3}]_0/[\mathbf{1a}]_0 > 10$. Thus, first-order rate constants k_{obs} could be derived from the decay curves by fitting the exponential function $A_t = A_0 \exp(-k_{obs}t) + C$, and second-order constants k_2 (Table 1) were obtained as the slopes of the linear relationships of k_{obs} vs $[\mathbf{3}]_0$ (see part 2 of the Supporting Information for details).

According to Equation (1), the nucleophile-specific parameters *N* (and s_N) of py-mNHO **1a** were obtained from the linear relationship of lg k_2 with the reported electrophilicities *E* of the reference compounds **3a–e** (R^2 = 0.9996, Figure S98, Supporting Information). With *N* = 26.16 (s_N = 0.52), py-mNHO **1a** is among the most reactive nucleophiles on the Mayr scale.[32e] Its reactivity is considerably higher than those of aryl-substituted triaz-mNHOs (**XI**; **XIII–XVI**)[13] and *N*-heterocyclic carbenes (NHCs)[34] and only exceeded by the entirely alkylated triaz-mNHOs **XVII** and **XVIII** (Figure 7).

Cheng and co-workers have shown that nucleophilicity and basicity of NHOs correlate only weakly.[11] Nevertheless, the Brønsted basicity of the new py-mNHO class and its nucleophilicity exceeds that of the recently reported triaz-mNHOs (*N*-Dipp).

The products of the reactions of py-mNHO **1a** with Michael acceptors **3c**, **4**, and **5** have been fully characterized (Scheme 3). Further, the reactions' DFT-calculated Gibbs energy profiles uniformly indicated stepwise mechanisms via rate-determining C–C bond formation between the exocyclic methylene unit of **1a** and the electrophilic centers of the Michael acceptors. Subsequently, the thus formed zwitter-

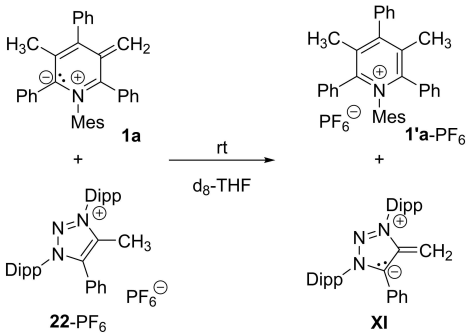

Scheme 6. Relative Brønsted basicity of py-mNHO **1a** and triaz-mNHO **XI**.

Table 1: Second-order rate constants k_2 for the reactions of py-mNHO **1a** with diethyl arylidenemalonates (reference electrophiles) in THF at 20 °C.

X–C_6H_4-CH=C(CO_2Et)$_2$	Mayr *E*	k_2 ($M^{-1}s^{-1}$)
3a (X = 4-CN)	−18.06	1.63×10^4
3b (X=H)	−20.55	8.17×10^2
3c (X = 4-Me)	−21.11	4.35×10^2
3d (X = 4-OMe)	−21.47	2.96×10^2
3e (X = 4-NMe_2)	−23.10	3.75×10^1

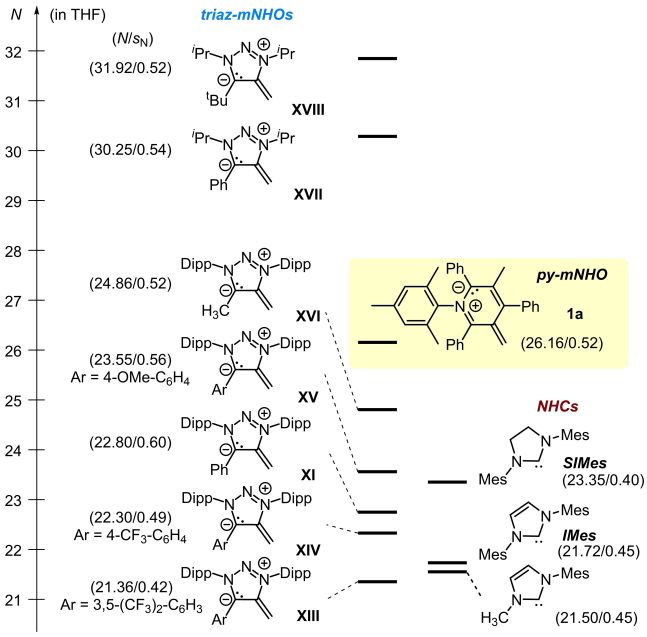

Figure 7. Mayr nucleophilicity scale for mNHOs and some NHCs.

ions may collapse via low barriers (or even barrierless) to give the isolated cyclic products (Figure 5 and Supporting Information). Given that Michael additions follow analogous mechanisms, we tested the predictive power of N (and s_N) of **1a** for reactions with the electrophiles **4** and **5**, which did not belong to the set of reference electrophiles used to derive the nucleophilicity parameter.

The comparison of k_2^{Eq1} values, calculated by using E, N, and s_N in equation (1), with experimentally determined second-order rate constants k_2^{exp} indicates for all investigated combinations of Michael acceptors with py-mNHO **1a** an accuracy of the predictions within approximately one order of magnitude (Table 2). Also, the reactivity of **1a** toward the heterocumulene PhNCNPh is well reflected by the Mayr reactivity parameters. We thus conclude that further reaction partners for the novel class of py-mNHOs can be selected by screening the various types of electrophiles in Mayr's reactivity database.[32,35,36,37]

In previous work, we have shown that the linear relationship of Mayr N parameters with a combination of quantum-chemically calculated methyl cation affinities (MCAs) and buried volumes (%V_{bur}) enables the prediction of the nucleophilicity of modified mNHO structures.[13] The corresponding data for py-mNHO **1a** (MCA = 512.5 kJ mol^{-1}; %V_{bur} = 34.7) matches very well with the existing correlation for triaz-mNHOs, and N of **1b–d** can be predicted straightforwardly, as depicted in Figure 8.

Table 2: Comparison of predicted and experimentally determined second-order rate constants k_2 for the reactions of py-mNHO **1a** with Michael acceptors (THF, 20 °C).

electrophile	Mayr E	k_2^{Eq1} ($M^{-1}s^{-1}$)	k_2^{exp} ($M^{-1}s^{-1}$)	k_2^{exp}/k_2^{Eq1}
acrylonitrile	−19.05[a]	4.98×10^3	1.84×10^4	3.7
PhNCNPh	−20.14[b]	1.35×10^3	2.10×10^3	1.6
t-butyl acrylate (**5**)	−20.22[a]	1.23×10^3	1.86×10^3	1.5
ethyl cinnamate (**4**)	−24.52[a]	7.13	7.93×10^1	11
cinnamonitrile (**11**)	−24.60[a]	6.47	6.52×10^1	10

[a] With E from ref. [36]. [b] With E from ref. [37].

Conclusion

We introduced non-stabilized (=CH_2) mesoionic *N*-heterocyclic olefins containing the pyridine heterocycle as a novel class of mesoionic compounds. Similar to previously described five-membered heterocyclic mesoionic methylides, the new olefins are strong carbon-based σ-donors. Additionally, they offer intriguing reactivity as 1,3-dipoles. Two 1,3-dipolar cycloaddition modes are accessible, which yield five-membered rings across the exocyclic methylene group and either the 4-position or the 2-position of the pyridinium core. In both cases, high diastereoselectivities were observed in reactions that formed up to three adjacent stereocenters in a single synthetic step. Quantum-chemical calculations show a dipolarophile-dependent gradual transition from stepwise to concerted mechanisms of the (3+2)-cycloadditions. Donor properties and nucleophilicities were determined based on TEP values and kinetic measurements, respectively, quantifying py-mNHOs as strong σ-donors and highly nucleophilic substrates on the Mayr reactivity scale.

This new class of carbon-centered, strong py-mNHO donors should enable applications in transition metal or main group chemistry as highly potent donor ligands or novel organocatalysts. The (3+2) cycloaddition mode could also be harnessed in organic synthesis, opening up synthetic pathways to complex bicyclic compounds. We are currently investigating the application of py-mNHOs for the activation of small inert molecules.

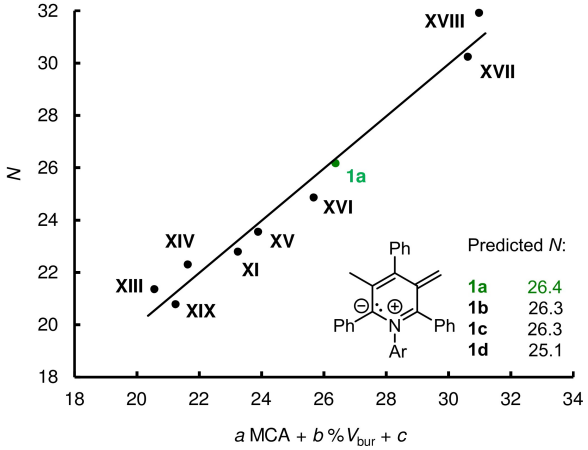

Figure 8. Correlation of experimental nucleophilicity N of mNHOs with a linear combination of MCA and %V_{bur} (data for **1a** from this work was not included when constructing the correlation line for the triazol-mNHOs **XI**; **XIII–XVIII**). For the structure of **XIX**, see SI.

Acknowledgements

We are grateful to Dr. Ljuba Iovkova, Dr. Julian Holstein, Dr. Christopher Golz, and David Mross for help with X-ray measurements and analysis and Max Amann for assistance with low-temperature NMR measurements. We thank the Deutsche Forschungsgemeinschaft (NMR: DFG project 452669591) under Germany's Excellence Strategy—EXC2033—project number 390677874-RESOLV. M.M.H. thanks the European Research Council, ERC-Starting grant "CC-CHARGED" (101077332) for financial support. This research was funded in part by the Austrian Science Fund (FWF), project no. J-4592 (Erwin Schrödinger fellowship to A.E.). For the purpose of open access, the author has applied a CC BY public copyright license to any Author Accepted Manuscript version arising from this submission. R.J.M. thanks the Deutsche Forschungsgemeinschaft for a fellowship (MA 9687/1-1) and Prof. Joseph Moran for support. Computations were performed at the High-Performance Computing Center of the University of Strasbourg. A part of the computing resources was funded by the Equipex Equip@Meso project (Programme Investissements d'Avenir) and the CPER Alsacalcul/Big Data. Open Access funding enabled and organized by Projekt DEAL.

Conflict of Interest

The authors declare no conflict of interest.

Data Availability Statement

The data that support the findings of this study are available in the supplementary material of this article.

Keywords: (3 + 2) Cycloaddition · Mesoions · N-Heterocyclic Olefins · Nucleophilicity · Ylides

[1] Reviews: a) J. Jacobs, E. Van Hende, S. Claessens, N. De Kimpe, *Curr. Org. Chem.* **2011**, *15*, 1340–1362; b) A. Kakehi, *Heterocycles* **2012**, *85*, 1529–1577; c) S. Sowmiah, J. M. S. S. Esperanca, L. P. Rebelo, C. A. M. Afonso, *Org. Chem. Front.* **2018**, *5*, 453–493; d) L. D. Funt, M. S. Novikov, A. F. Khlebnikov, *Tetrahedron* **2020**, *76*, 131415; e) S. Dong, X. Fu, X. Xu, *Asian J. Org. Chem.* **2020**, *9*, 1133–1143; f) A. Rajmane, A. Kumbhar, *Chem. Papers*, **2023**, https://doi.org/10.1007/s11696-023-03056-z.

[2] X. M. Zhang, F. G. Bordwell, M. Van Der Puy, H. E. Fried, *J. Org. Chem.* **1993**, *58*, 3060–3066.

[3] D. S. Allgäuer, P. Mayer, H. Mayr, *J. Am. Chem. Soc.* **2013**, *135*, 15216–15224.

[4] For selected examples, see: a) D. Shen, W. Jin, Y. Bai, Y. Huang, H. Lyu, L. Zeng, M. Wang, Y. Tang, W. Wan, X. Dong, Z. Gao, H.-L. Piao, X. Liu, Y. Liu, *Angew. Chem. Int. Ed.* **2021**, *60*, 16067–16076; b) F. Meng, S. Bi, Z. Sun, B. Jiang, D. Wu, J.-S. Chen, F. Zhang, *Angew. Chem. Int. Ed.* **2021**, *60*, 13614–13620; c) A. Saady, P. Sudhakar, M. Nassir, A. Gedanken, *Ultrason. Sonochem.* **2020**, *67*, 105182; d) M. Kang, C. Zhou, S. Wu, B. Yu, Z. Zhang, N. Song, M. Mei Suet Lee, W. Xu, F.-J. Xu, D. Wang, L. Wang, B. Zhong Tang, *J. Am. Chem. Soc.* **2019**, *141*, 16781–16789; e) X. Xie, M. Zuffo, M.-P. Teulade-Fichou, A. Granzhan, *Beilstein J. Org. Chem.* **2019**, *15*, 1872–1889.

[5] A few reactions of 2-methylene-1,2-dihydropyridines were reported in: a) H.-G. Henning, L. H. Thanh, J. Laue, B. Urban, G. Reck, *Monatsh. Chem.* **1994**, *125*, 95–105; b) A. Fürstner, M. Alcarazo, R. Goddard, C. W. Lehmann, *Angew. Chem. Int. Ed.* **2008**, *47*, 3210–3214; c) X. Zhang, L. Wang, Q. Wang, F. Ge, X. Wuang, *ChemistrySelect* **2019**, *4*, 8655–8660; d) J. Reitz, P. W. Antoni, J. J. Holstein, M. M. Hansmann, *Angew. Chem. Int. Ed.* **2023**, *62*, e202301486.

[6] For an overview on mesoions, see: a) W. D. Ollis, S. P. Stanforth, C. A. Ramsden, *Tetrahedron* **1985**, *41*, 2239–2329; b) A. Schmidt, S. Wiechmann, C. F. Otto, *Adv. Heterocycl. Chem.* **2016**, *119*, 143–172; c) C. A. Ramsden, in *Heterocyclic Mesomeric Betaines and Mesoionic Compounds*, *Adv. Heterocycl. Chem. Vol. 137*, Elsevier, Amsterdam, **2022**; d) A. R. Katritzky, N. Dennis, *Chem. Rev.* **1989**, *89*, 827–861.

[7] a) According to IUPAC (ref. [7b]), mesoionic compounds are currently defined as "Dipolar five- (possibly six-) membered heterocyclic compounds in which both the negative and the positive charge are delocalized, for which a totally covalent structure cannot be written, and which cannot be represented satisfactorily by any one polar structure. The formal positive charge is associated with the ring atoms, and the formal negative charge is associated with ring atoms or an exocyclic nitrogen or chalcogen atom. Mesoionic compounds are a subclass of betaines." Based on the mesoionic compounds with exocyclic nitrogen or oxygen atoms, which are covered by this definition, we adopted the nomenclature analogously for mesoionic methylides, in which the formal negative charge is associated with an exocyclic carbon atom; b) *IUPAC Compendium of Chemical Terminology*, 3rd ed. International Union of Pure and Applied Chemistry, **2006**. Online version 3.0.1, 2019. https://doi.org/10.1351/goldbook.M03842; For selected reports on six-membered heterocyclic mesoionic compounds, see: c) R. M. Moriarty, J. M. Kliegman, R. B. Desai, *Chem. Commun.* **1967**, 1045–1046; d) J. Honzl, M. Šorm, V. Hanuš, *Tetrahedron* **1970**, *26*, 2305–2319; e) H. Hagemann, K. Ley, *Angew. Chem. Int. Ed. Engl.* **1972**, *11*, 1012–1013.

[8] M. M. Hansmann, P. W. Antoni, H. Pesch, *Angew. Chem. Int. Ed.* **2020**, *59, 5782–5787*.

[9] S. Wang, C. Zhang, D. Li, Y. Zhou, Z. Su, X. Feng, S. Dong, *Sci. China Chem.* **2023**, *66*, 147–154.

[10] I. Berg, L. Schio, J. Reitz, E. Molteni, L. Lahav, C. G. Bolanos, A. Goldoni, C. Grazioli, G. Fratesi, M. M. Hansmann, L. Floreano, E. Gross, *Angew. Chem. Int. Ed.* **2023**, *62*, e202311832.

[11] Z. Li, P. Ji, J.-P. Cheng, *J. Org. Chem.* **2021**, *86*, 2974–2985.

[12] For selected reviews on NHOs, see: a) R. D. Crocker, T. V. Nguyen, *Chem. Eur. J.* **2016**, *22*, 2208–2213; b) M. M. D. Roy, E. Rivard, *Acc. Chem. Res.* **2017**, *50*, 2017–2025; c) S. Naumann, *Chem. Commun.* **2019**, *55*, 11658–11670; d) Q. Liang, D. Song, *Dalton Trans.* **2022**, *51*, 9191–9198; e) M. G. D. Sharma, R. Dandela, V. Dhayalan, *Chem. Eur. J.* **2023**, e202302106.

[13] A. Eitzinger, J. Reitz, P. W. Antoni, H. Mayr, A. R. Ofial, M. M. Hansmann, *Angew. Chem. Int. Ed.* **2023**, *62*, e202309790.

[14] a) P. W. Antoni, J. Reitz, M. M. Hansmann, *J. Am. Chem. Soc.* **2021**, *143*, 12878–12885; b) P. W. Antoni, C. Golz, J. J. Holstein, D. A. Pantazis, M. M. Hansmann, *Nat. Chem.* **2021**, *13*, 587–593; For a minireview, see: c) M. M. Hansmann, *Angew. Chem. Int. Ed.* **2023**, *62*, e202304574.

[15] a) Z. Zhang, S. Huang, L. Huang, X. Xu, H. Zhao, X. Yan, *J. Org. Chem.* **2020**, *85*, 12036–12043; b) S. Maji, A. Das, S. K. Mandal, *Chem. Sci.* **2021**, *12*, 12174–12180.

[16] A. Merschel, Y. V. Vishnevskiy, B. Neumann, H.-G. Stammler, R. S. Ghadwal, *Dalton Trans.* **2022**, *51*, 8217–8222.
[17] For the reactivity of substituted (=CHR) mNHOs, see: a) Q. Liang, Y. Zeng, P. A. M. Ocampo, H. Zhu, Z.-W. Qu, S. Grimme, D. Song, *Chem. Commun.* **2023**, *59*, 4770–4773; b) Q. Liang, H. Hayashi, L. Li, D. Song, *Chem. Commun.* **2021**, *57*, 10927–10930.
[18] For acceptor substituted quinolium based mesoions or related substituted systems, see: a) A. Schmidt, S. Batsyts, A. Smeyanov, T. Freese, E. G. Hübner, M. Nieger, *J. Org. Chem.* **2016**, *81*, 4202–4209; b) S. Sangher, C. Kesornpun, T. Aree, C. Mahidol, S. Ruchirawat, P. Kittakoop, *Dyes Pigm.* **2020**, *178*, 108341; c) Y. Yang, M. Xu, D. Song, *Chem. Commun.* **2015**, *51*, 11293–11296; d) M. Cheng, D. Lu, Y.-S. Ding, Q.-X. Jia, *Z. Anorg. Allg. Chem.* **2015**, *641*, 1969–1973.
[19] For acceptor-stabilized systems, see: a) S. Mummel, F. Lederle, E. Hübner, J. C. Namyslo, M. Nieger, A. Schmidt, *Angew. Chem. Int. Ed.* **2021**, *60*, 18882–18887; b) S. Araki, J. Mizuya, Y. Butsugan, *Chem. Lett.* **1984**, *13*, 1045–1046.
[20] Though the pyridine carbenes **IV**–**VII** could not be isolated, several groups reported the corresponding metalated pyridine complexes: a) E. Stander-Grobler, O. Schuster, G. Heydenrych, S. Cronje, E. Tosh, M. Albrecht, G. Frenking, H. G. Raubenheimer, *Organometallics* **2010**, *29*, 5821–5833; b) S. K. Schneider, G. R. Julius, C. Loschen, H. G. Raubenheimer, G. Frenking, W. A. Herrmann, *Dalton Trans.* **2006**, 1226–1233; c) O. Schuster, L. Yang, H. G. Raubenheimer, M. Albrecht, *Chem. Rev.* **2009**, *109*, 3445–3478; d) A. Vivancos, C. Segarra, M. Albrecht, *Chem. Rev.* **2018**, *118*, 9493–9586.
[21] For relative deuterium exchange rates of *N*-methyl pyridinium ions in aqueous solutions, see: a) Y. Kawazoe, M. Ohnishi, Y. Yoshioka, *Chem. Pharm. Bull.* **1967**, *15*, 1225–1231; b) J. A. Zoltewicz, R. E. Cross, *J. Chem. Soc. Perkin Trans. 2* **1974**, 1363–1368.
[22] a) E. D. Glendening, F. Weinhold, *J. Comput. Chem.* **1998**, *19*, 593–609; b) E. D. Glendening, F. Weinhold, *J. Comput. Chem.* **2013**, *34*, 1429–1437.
[23] A. Stanger, *Eur. J. Org. Chem.* **2020**, 3120–3127.
[24] We utilized a similar homodesmotic Scheme as proposed by Champagne and Houk for mesoionic azomethine ylides: P. A. Champagne, K. N. Houk, *J. Org. Chem.* **2017**, *82*, 10980–10988.
[25] J. Fortage, C. Peltier, C. Perruchot, Y. Takemoto, Y. Teki, F. Bedioui, V. Marvaud, G. Dupeyre, L. Pospísil, C. Adamo, M. Hromadová, I. Ciofini, P. P. Lainé, *J. Am. Chem. Soc.* **2012**, *134*, 2691–2705.
[26] Deposition numbers 2310205 (for **(1b)$_2$**), 2310213 (for **1a**), 2310215 (for **1b**), 2310209 (for **1b**), 2310202 (for **2**), 2310212 (for **6a**), 2310211 (for **6b**), 2310207 (for **9**), 2310203 (for **10**), 2310206 (for **12**), 2310200 (for **13**), 2310204 (for **15**), 2310201 (for **17**), 2310210 (for **20a**), 2310208 (for **20b**), and 2310214 (for **21**) contain the supplementary crystallographic data for this paper. These data are provided free of charge by the joint Cambridge Crystallographic Data Centre and Fachinformationszentrum Karlsruhe Access Structures service.
[27] Slight amounts of KHMDS can isomerize **9** to give a mixture of **9** and **10**.
[28] Computations indicate this mechanism to be implausible at −40 °C, and it is likely that some traces of unknown catalyst are involved.
[29] a) R. E. Lyle, G. J. Gauthier, *Tetrahedron Lett.* **1965**, 4615–4621; b) G. Doddi, G. Ercolani, P. Mencarelli, *J. Org. Chem.* **1992**, *57*, 4431–4434.
[30] For a review on the history of 1,3-dipolar cycloadditions (Huisgen reactions), see: M. Breugst, H.-U. Reissig, *Angew. Chem. Int. Ed.* **2020**, *59*, 12293–12307.
[31] H. V. Huynh, *Chem. Rev.* **2018**, *118*, 9457–9492.
[32] a) H. Mayr, M. Patz, *Angew. Chem. Int. Ed.* **1994**, *33*, 938–957; b) H. Mayr, T. Bug, M. F. Gotta, N. Hering, B. Irrgang, B. Janker, B. Kempf, R. Loos, A. R. Ofial, G. Remennikov, H. Schimmel, *J. Am. Chem. Soc.* **2001**, *123*, 9500–9512; c) H. Mayr, B. Kempf, A. R. Ofial, *Acc. Chem. Res.* **2003**, *36*, 66–77; d) H. Mayr, A. R. Ofial, *SAR QSAR Environ. Res.* **2015**, *26*, 619–646; e) the database of Mayr reactivity parameters (N, s_N, and E) is freely accessible at www.cup.lmu.de/oc/mayr/reaktionsdatenbank2/, (accessed 12th Dec, 2023).
[33] O. Kaumanns, R. Lucius, H. Mayr, *Chem. Eur. J.* **2008**, *14*, 9675–9682.
[34] a) B. Maji, M. Breugst, H. Mayr, *Angew. Chem. Int. Ed.* **2011**, *50*, 6915–6919; b) A. Levens, F. An, M. Breugst, H. Mayr, D. W. Lupton, *Org. Lett.* **2016**, *18*, 3566–3569.
[35] Our attempts to determine k_2^{exp} for the reaction **1a** + diethyl maleate (**7**) failed, however. The non-linearity of the k_{obs} vs [**7**] plots indicated higher order kinetics, which was not further explored in this study.
[36] a) D. S. Allgäuer, H. Jangra, H. Asahara, Z. Li, Q. Chen, H. Zipse, A. R. Ofial, H. Mayr, *J. Am. Chem. Soc.* **2017**, *139*, 13318–13329; b) R. J. Mayer, P. W. A. Allihn, N. Hampel, P. Mayer, S. A. Sieber, A. R. Ofial, *Chem. Sci.* **2021**, *12*, 4850–4865.
[37] Z. Li, R. J. Mayer, A. R. Ofial, H. Mayr, *J. Am. Chem. Soc.* **2020**, *142*, 8383–8402.

Manuscript received: November 29, 2023
Accepted manuscript online: December 28, 2023
Version of record online: January 18, 2024